Scattering of EM waves from a Rotating Dispersive Very Good Conducting Cylinder

Esmail M M Abuhduma
Computer Science, Physics and
Engineering
Benedict College
Coulmbia, USA
esmail.abuhdima@benedict.edu

Ashleigh Reeves
Computer Science, Physics and
Engineering
Benedict College
Coulmbia, USA
Ashleigh.reeves60@my.benedict.edu

Gurcan Comert
Computer Science, Physics and
Engineering
Benedict College
Coulmbia, USA
gurcan.comert@benedict.edu

Williams Kellen
Computer Science, Physics and
Engineering
Benedict College
Coulmbia, USA
kellen.williams97@my.benedict.edu

Ahmed Elqaouaq
Computer Science, Physics and
Engineering
Benedict College
Coulmbia, USA
ahmed.el-qaouaq@my.benedict.edu

Abstract— This research focuses on studying the scattering phenomenon. Scattering electromagnetic waves from a rotating conducting cylinder is investigated when the material of the conducting cylinder is linear, homogeneous, isotropic, and dispersive. This study is an extension of a previous work that investigated the effect of the rotating conducting cylinder on the scattered phase and amplitude, when the material of the conducting cylinder is linear, homogeneous, isotropic, and nondispersive. One of the important result of the previous work is that the Franklin transformation is a proper and more accurate method to calculate the effect of the rotation, and gives more accurate results than Galilean transformation. In this research, the Franklin transformation will be used to investigate the effect of the rotation of the object on the scattered phase and magnitude of the incident waves. The two types of incident waves (E-wave and H-wave) will be considered herein. The simulation results will clearly display the behavior of the scattered phase and magnitude with changes to the incident frequency, the speed of rotation, and the radius of the very good conducting cylinder. Moreover, this result is compared with the result of the previous work (non- dispersive material) to show the behavior of the scattered phase and magnitude when the incident frequency, speed of the rotation and radius of the very good conducting cylinder is changed.

Keywords—rotating, scattered field, dispersive, nondispersive, scattered phase, scattered amplitude

I. INTRODUCTION (HEADING 1)

This work sustains past efforts that investigated the effects of the rotation of the very good conducting cylinder on the scattered phase and magnitude [1]. The material of the very good conducting cylinder was linear, homogeneous, isotropic, and nondispersive. In other words, the constitutive parameters of the conducting material, permittivity (\mathcal{E}) , permeability

 (μ) , and conductivity (σ) are not functions of the applied field, the position, the direction of the applied field, and the frequency[2]. This simulation helps to create a new model to simulate the effect of rotation of the complex object on the scattered field. This model is used to develop the capability of the radar system to create accurate information about the scatterer [3]. In this paper, the Franklin transformation is used

to calculate the constitutive relations in the instantaneous frame (rotating frame) [4]. It is considered that the material of the very good conducting cylinder is linear, homogeneous, isotropic, and dispersive. Dispersive means the constitutive parameters are changed when the incident frequency is changed. The only one change in the properties of the very good conducting material in comparison with the previous work is that the constitutive parameters $\varepsilon(\omega)$, $\mu(\omega)$, and $\sigma(\omega)$ are a function of the incident frequency. The Drude model is used to determine the relative permittivity $\varepsilon_r(\omega)$, the relative permeability $\mu_r(\omega)$, the conductivity $\sigma(\omega)$, and the refractive index $n(\omega)$ [5]. Finally, the simulation result is compared with the previous result to see the effect of the dispersive conducting material on the scattered phase and magnitude.

II. SCATTERING FIELDS

In this section, the scattering of both types of polarization of the incident waves (E- wave and H-wave) from a rotating very good conducting cylinder are investigated. The accurate method to find relation between fields in the laboratory frame and the rotating frame is Franklin transformation that is defined as [4]

$$r' = r$$
, $\phi' = \phi \cosh(\beta) - \frac{ct}{r} \sinh(\beta)$, (1)

$$z' = z$$
, $t' = t \cosh(\beta) - \frac{r\phi}{c} \sinh(\beta)$, (2)

where $\beta = \Omega \, r/c$, c is speed of light, Ω is the angular velocity, and r is the radius of the very good conducting cylinder. The constitutive relations in the instantaneous inertial frame are defined as

$$D' = \varepsilon(\omega)E' \tag{3}$$

$$B' = \mu(\omega)H' \tag{4}$$

$$J' = \sigma(\omega)E', \tag{5}$$

where E, H, D, B, and J are the electric field, the magnetic field, the electrical flux density, the magnetic flux density and the current density respectively. The Drude model defined the complex permittivity, the complex permeability, the complex conductivity, and the complex refractive index as following

$$\varepsilon_r(\omega) = 1 - \frac{\omega p^2}{\omega^2 + i\omega\Gamma},\tag{6}$$

$$\mu_r(\omega) = 1 + \frac{\omega p^2}{j\omega(j\omega + \Gamma)},\tag{7}$$

$$\sigma(\omega) = \varepsilon_o \frac{\omega p^2}{-j\omega + \Gamma} = \frac{nq^2}{m_c \Gamma}, \tag{8}$$

$$n(\omega)^2 = 1 + j \frac{\sigma(\omega)}{\omega \varepsilon_o}, \tag{9}$$

where $\omega p^2 = \frac{nq^2}{m \, \varepsilon}$, m_e is the mass of the charge, q is

the amount of the charge, \mathcal{E}_o is the vacuum electric permittivity, and Γ is the damping coefficient. The corresponding constitutive relations in the laboratory frame

$$(1-n^2s^2)D_r = \varepsilon(\omega)(1-s^2)E_r + s(n^2-1)H_z, \quad (10)$$

$$(1-n^2s^2)D_z = \varepsilon(\omega)(1-s^2)E_z + s(n^2-1)H_r, \quad (11)$$

$$(1-n^2s^2)B_r = \mu(\omega)(1-s^2)H_r + s(n^2-1)E_z$$
, (12)

$$(1 - n^2 s^2) B_z = \mu(\omega) (1 - s^2) H_z + s(n^2 - 1) E_r, (13)$$

$$J_z = \sigma(\omega)\gamma(E_z - s\mu(\omega)B_r), \tag{14}$$

$$J_r = \sigma(\omega)\gamma(E_r + \mu(\omega)sB_z), \qquad (15)$$

$$J_{\omega} = \sigma(\omega) \gamma^{-1} E_{\omega} \tag{16}$$

where $s = \tanh(\beta)$, $\gamma = \lceil 1 - s^2 \rceil^{-0.5}$, and $n^2 = \varepsilon \mu$.

A. E-wave (TM mode)

In the case of the E-wave, the geometry of the rotating very good conducting cylinder is shown in the fig. 1. It is shown

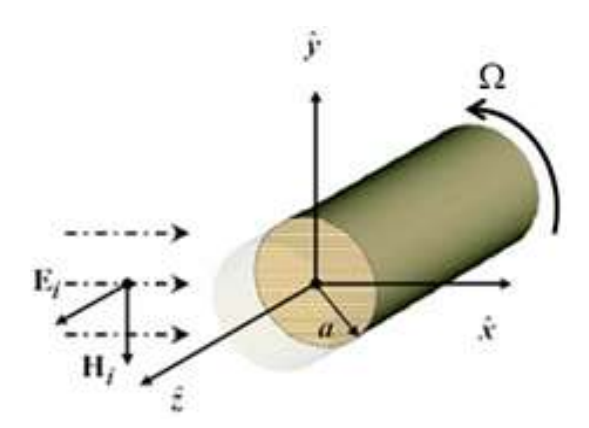


Fig. 1 Scattering of E-wave

that the direction of the electric filed is parallel to the axes of rotation of the very good conducting cylinder. Since the direction of the incident wave is in x-axes, so the magnetic component is in negative y-axes. The incident electric field is given by [6]

$$E_z^i = e^{-jkx} = \sum_{-\infty}^{+\infty} j^{-n} J_n(kr) e^{jn\varphi},$$
 (17)

 $k = \omega/c$ is the wave number. The form of the Maxwell's equations inside the conducting cylinder are written as

$$\frac{c}{r}\frac{\partial E_z}{\partial \varnothing} = -j\omega B_r,\tag{18}$$

$$\frac{\partial E_z}{\partial r} = j\omega c^{-1} B_{\varphi},\tag{19}$$

$$\frac{c}{r}\frac{\partial \left(rH_{\varnothing}\right)}{\partial r} - \frac{c}{r}\frac{\partial H_{r}}{\partial \varnothing} = j\omega D_{z} + J_{z}. \tag{20}$$
Substituting (10)-(14) into (18)-(20) gives

$$\frac{1}{r}\frac{\partial}{\partial r}\left(r\frac{\partial E_z}{\partial r}\right) + \left(\gamma_n^2 - \frac{n^2}{r^2}\right)E_z = 0, \quad (21)$$

where
$$\gamma_n^2 = k^2 N^2 (1 - jq) + \frac{n\omega\Omega}{c^2} (2N^2 - 2 - jN^2q)$$
.

Equation (21) is known a Bessel type equation and its solution is given as[7]

$$E_z = \sum_{-\infty}^{+\infty} A_{en} J_n (\gamma_n r) e^{jn\varphi}, \qquad (22)$$

where E_{z} the electric field inside the very good conducting cylinder and A_{en} is the constant coefficient. The scattered electric field can be written as

$$E_z^{sc} = \sum_{-\infty}^{+\infty} B_{en} H_n^{(2)} (kr) e^{jn\varphi}, \qquad (23)$$

where B_{en} is the scattered coefficient. The boundary conditions are applied at r = a to find the unknown coefficients as following [8]

$$\left(E_z^{sc} + E_z^i - E_z\right) = 0, \qquad (24)$$

$$\left(H_{\varphi}^{sc} + H_{\varphi}^{i} - H_{\varphi}\right) = 0. \tag{25}$$

Combining (17), (22), and (23) with the Maxwell's equations in the laboratory frame gives

$$B_{en}H_n^{(2)}(kr)+j^{-n}J_n(ka)-A_{en}J_n(\gamma_n r)=0$$
, (26)

$$kB_{en}H_{n}^{\prime(2)}(Ka)+kj^{-n}J_{n}(Ka)-cA_{en}\gamma_{n}J_{n}(\gamma_{n}a)=0. (27)$$

Solving (26) and (27) for B_{en} and A_{en} yields

$$B_{en} = \frac{j^{-n} \left[c \gamma_n J_n'(\gamma_n a) J_n(ka) - k J_n(\gamma_n a) J_n'(Ka) \right]}{k J_n(\gamma_n a) H_n'^{(2)}(Ka) - c \gamma_n J_n'(\gamma_n a) H_n^{(2)}(ka)}, \quad (28)$$

$$A_{en} = \frac{j^{-n}k \left[J_n'(ka) H_n^{(2)}(ka) - J_n(ka) H_n'^{(2)}(Ka) \right]}{c\gamma_n J_n'(\gamma_n a) H_n^{(2)}(ka) - k J_n(\gamma_n a) H_n'^{(2)}(Ka)}. (29)$$

In the case of the TM mode, the scattering coefficient that is defined by (28) does not function on the angular velocity Ω . In other words, the scattering of the rotating very good conducting cylinder is similar to the stationary case.

B. H-wave (TE mode)

In this case, the axes of rotation of the very good conducing cylinder is z-axes as shown in Fig. 2. It is seen that the direction of the component of the magnetic field is parallel to the axes of rotation. According to the Maxwell's equations,

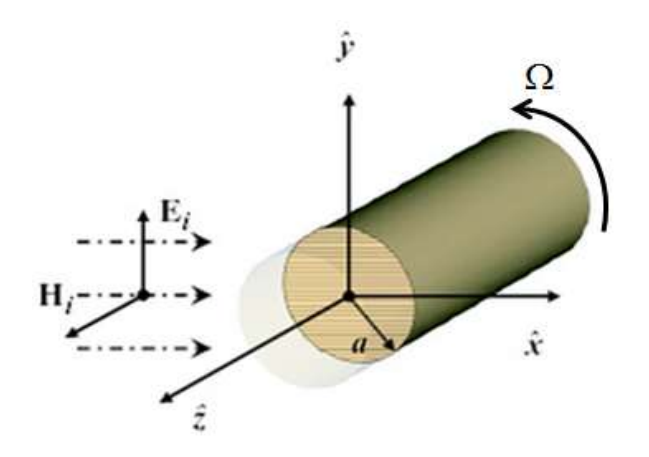


Fig. 2 Scattering of H-wave

the direction of the electric field is in y-axes because the direction of the propagating wave is in x-axes. The incident magnetic field is given by

$$H_z^i = e^{-jkx} = \sum_{-\infty}^{+\infty} j^{-n} J_n(kr) e^{jn\varphi}$$
. (30)

Maxwell's equations are defined as [9]

$$\frac{c}{r}\frac{\partial H_z}{\partial \varnothing} = J_r + j\omega D_r, \qquad (31)$$

$$-c\frac{\partial H_z}{\partial r} = J_{\varphi} + j\omega D_{\varphi}, \qquad (32)$$

$$\frac{c}{r}\frac{\partial(rE_{\varphi})}{\partial r} - \frac{c}{r}\frac{\partial E_{r}}{\partial \varphi} = -j\omega B_{z}.$$
 (33)

Substitution (10)-(16) into (30)-(33) gives

$$\frac{1}{r}\frac{\partial}{\partial r}\left(r\frac{\partial H_z}{\partial r}\right) + \left[\gamma_n^2 - \frac{n}{r^2}\right]H_z = 0, \quad (34)$$

where $\gamma_n^2 = k^2 N^2 (1 - jq) + \frac{n\omega\Omega}{c^2} (2N^2 - 2 - jN^2q)$

Equation (34) is the Bessel type, so its solution is [7]

$$H_Z = \sum_{-\infty}^{+\infty} A_{hn} J_n (\gamma_n r) e^{jn\varphi}, \qquad (35)$$

where A_{hn} is the constant coefficient. The scattered magnetic field is found as

$$H_z^{sc} = \sum_{n=0}^{+\infty} B_{hn} H_n^{(2)} (kr) e^{jn\varphi}$$
 (36)

where B_{hn} is the scattering coefficient. The unknown coefficients are determined by using boundary conditions as

$$\left(E_{\varphi}^{i} + E_{\varphi}^{sc} - E_{\varphi}\right)_{a} = 0, \tag{37}$$

$$\left(H_z - H_z^i - H_z^{sc}\right)_a = c\rho_s \tanh\beta, \qquad (38)$$

where ρ_s is surface charge density. Substituting (30), (35), and (36) into (37) and (38) gives

$$-k \ j^{-n} J_n'(ka) - k B_{hn} H_n'^{(2)}(ka) + \frac{c}{\alpha^2 \epsilon_r} \gamma_n A_{hn} J_n'(\gamma_n a) = 0, (39)$$

$$A_{hn} \left[1 + \frac{cs}{\omega \alpha^2 a} \mathbf{n} \right] J_n \left(\gamma_n a \right) - j^{-n} \left[1 + \frac{s}{\omega a \epsilon_n} \mathbf{n} \right] J_n \left(ka \right) - B_{hn} \left[1 + \frac{s}{\omega a \epsilon_n} \mathbf{n} \right] H_n^{(2)} \left(ka \right) = 0$$
 (40)

When (39) and (40) are solved for B_{hn} and A_{hn} , the final solution is

$$B_{ba} = \frac{j^{-n} \left[k J_n'(ka) J_n(\gamma_a a) \left(\alpha^2 \epsilon_r(\omega) + n \frac{\Omega \epsilon_r(\omega)}{\omega} \right) - c \gamma_n J_n(ka) J_n'(\gamma_a a) \left(1 + n \frac{\Omega}{\omega c \epsilon_o} \right) \right]}{c \gamma_n J_n'(\gamma_a a) H_n^{(2)}(Ka) \left(1 + n \frac{\Omega}{\omega c \epsilon_o} \right) - k J_n(\gamma_a a) H_n^{(2)}(ka) \left(\alpha^2 \epsilon_r(\omega) + n \frac{\Omega \epsilon_r(\omega)}{\omega} \right)}$$
(41)

$$A_{hn} = \frac{\int_{n}^{-n} \left[J_{n}(ka) H_{n}^{(2)}(ka) \left(\left(1 + n \frac{\Omega}{\omega c \epsilon_{o}} \right) \right) - J_{n}(ka) H_{n}^{(2)}(Ka) \left(1 + n \frac{\Omega}{\omega c \epsilon_{o}} \right) \right]}{H_{n}^{(2)}(ka) - J_{n}(\gamma_{n}a) H_{n}^{(2)}(Ka) \left(1 + n \frac{\Omega}{\omega c \epsilon_{o}} \right) \left(\frac{c \gamma_{n}}{k\alpha^{2} \epsilon_{r}(\omega)} \right)}$$

$$(42)$$

In the case of H-wave, the angular velocity Ω showed up in the terms of the scattering coefficient B_{hn} as shown in (41). It can be concluded that the effect of the rotation on the scattered fields is more evident in the case of H-wave than E-wave.

III. SIMULATION RESULT

In this section, the pattern of the phase and magnitude of the backscattered fields are shown in both polarizations when the frequency of the incident waves is varied at different values of $\beta_a = \frac{\Omega a}{c}$ and a. Also, these simulation results are compared with the previous results to see the effect of the characteristics of the material of the rotating very good conducting cylinder on the scattered phase and magnitude.

A. TM mode

The backscattered electric field in the far field region is define by

$$E_z^{sc} = \frac{1}{\sqrt{k\pi}} \sum_{-\infty}^{+\infty} j^n \left(1 + j\right) B_{en} e^{jn\pi} , \qquad (43)$$

where B_{en} is the scattering coefficient and given by (28). It is clearly seen that the backscattered phase and magnitude of the rotation case is similar to the stationary case as show in Fig. 3 and 4. It can be said that the effect of rotating the very good conducting cylinder in the case of dispersive material is vanished in the case of E-wave. In comparison with previous work (non-dispersive material), the scattered field is not affected by the rotation of the very good conducting cylinder. That means both cases (dispersive, and non-dispersive) give a similar result.

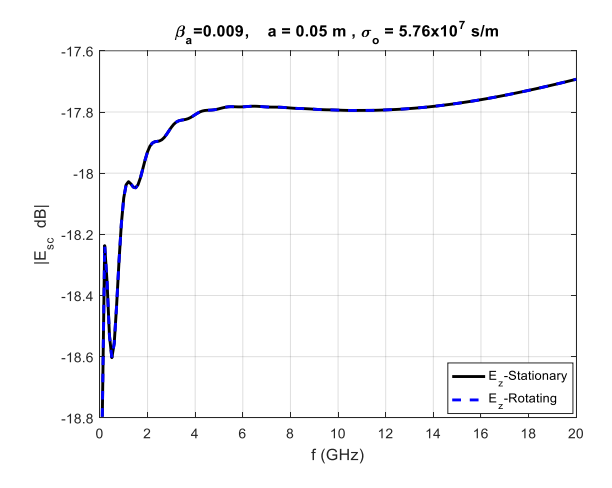


Fig. 3 Magnitude of the backscattered electric field

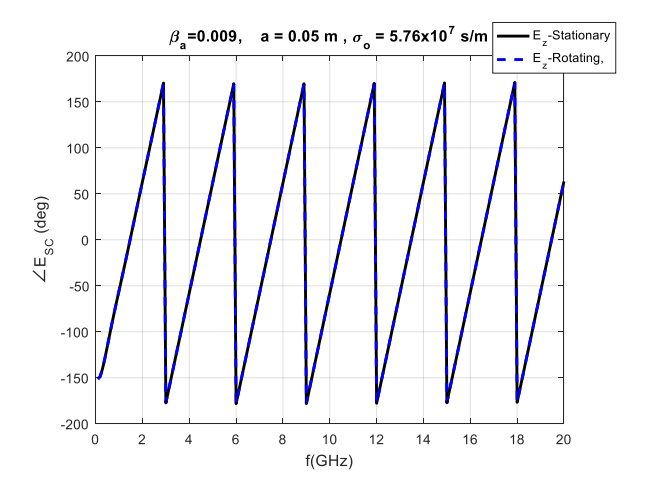


Fig. 4 Phase of the backscattered Electric field

B. TE mode

In the case of H-wave, the far magnetic field is written as

$$H_z^{sc} = \frac{1}{\sqrt{k\pi}} \sum_{-\infty}^{+\infty} j^n \left(1 + j\right) B_{hn} e^{jn\pi} , \qquad (44)$$

where B_{hn} is the scattering coefficient and defined by (41). The simulation result shows that the backscattered phase and magnitude are affected by the rotation of the very good conducting cylinder. Figs. 5 and 7 show periodic pulses during the rotation of the conducting cylinder. Equation (41) shows that the scattering coefficient B_{hn} depends upon the rotation velocity Ω and the radius of the cylinder a. When a0 and a1 and a3, the period of the pulses is 3GHz as shown in Fig. 5. When the speed of rotation is increased a1 as shown in Fig. 5. In contrary, the period of these periodic pulses is decreased when the radius

of the very good conducting cylinder is increased as shown in Figs. 7 and 9. When $\beta_a=0.009$ and a=0.09m, the period of the pulses is 1.8 GHz as shown in Fig. 7. The peaks of the pulses approached 0.8 GHz when the radius (a) is increased to 0.2m. The backscattered phase of the rotation case shows a similar pattern to the backscattered magnitude as shown in Figs. 6, 8, and 10. In other words, the backscattered phase shows a periodic pulse in comparison with stationary case. It is found that the relation between the

rotation frequency
$$\left(f_r = \frac{\Omega}{2\pi}\right)$$
 and the period frequency

$$\left(f_p\right)$$
 is equal to $\frac{f_r}{f_p} = \frac{\beta_a c}{2\pi f_p a} = 0.0026$. This ratio is

unique for this kind of dispersive material. In comparison with the previous result (non-dispersive), the backscattered phase and magnitude was affected by the rotation [10]. This effect is shown as a sinusoidal behavior of the backscattered phase. The period of this sinusoidal pattern is decreased when the rotation of the very good conducting cylinder is increased. Also, the backscattered magnitudes showed a periodicity, especially in higher frequencies.

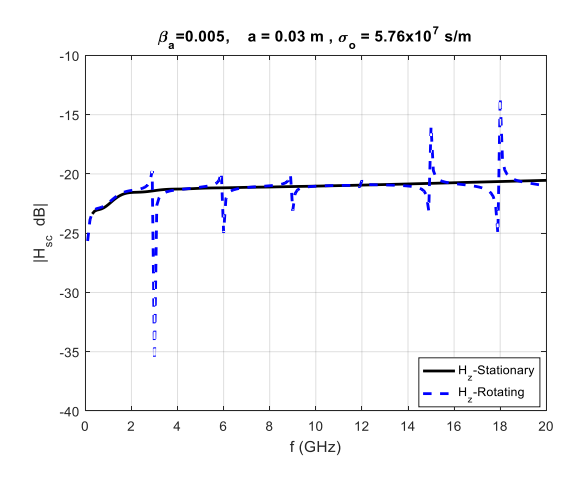


Fig. 5 Magnitude of the backscattered magnetic field

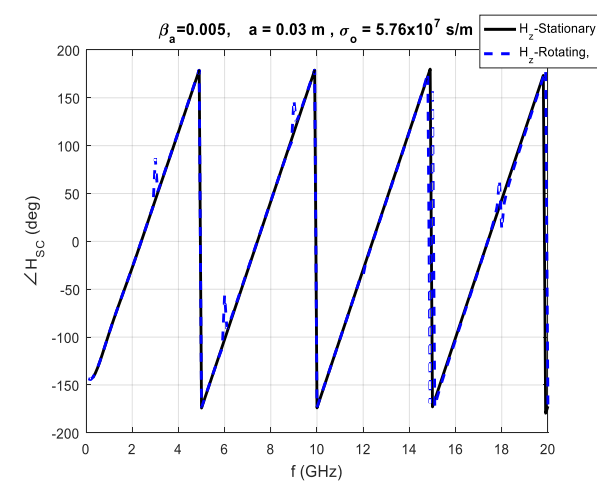


Fig. 6 Phase of the backscattered magnetic field

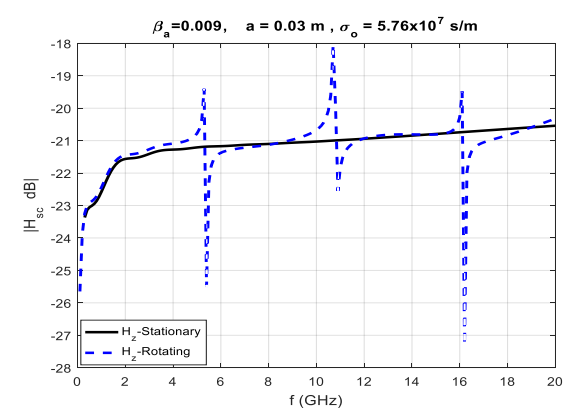


Fig. 7 Magnitude of the backscattered magnetic field

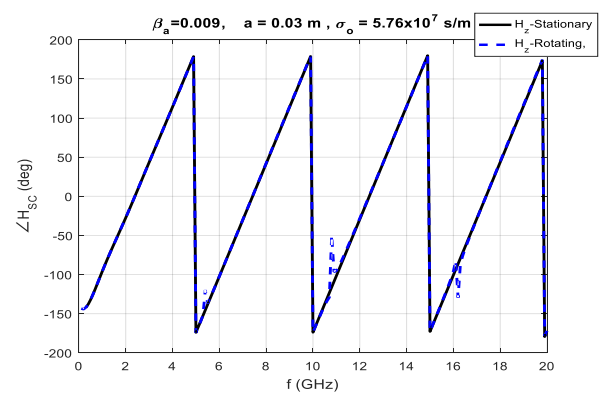


Fig. 8 Phase of the backscattered magnetic field

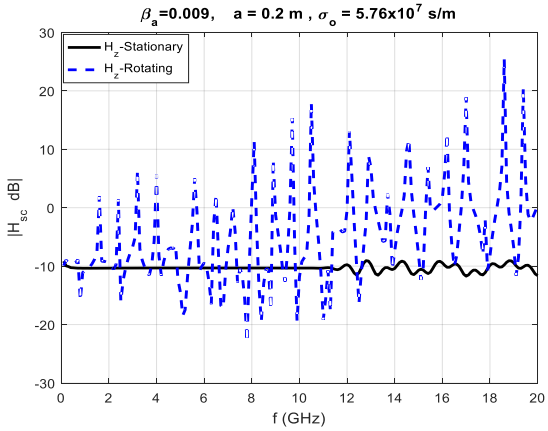


Fig. 9 Magnitude of the backscattered magnetic field

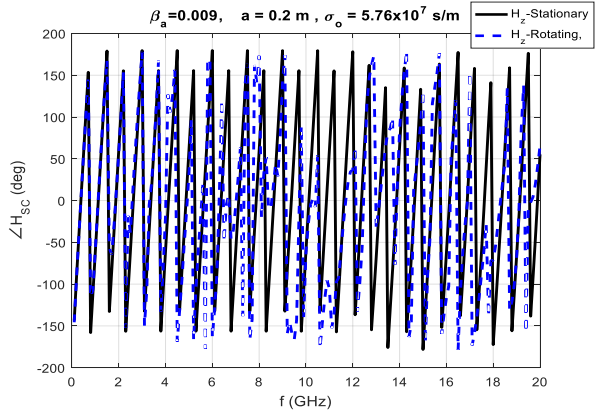


Fig. 10 Phase of the backscattered magnetic field

The magnitude of the backscattered field is generated with $\beta_a=0.009$, $f=6.45\,GHz$, $a=0.05\,m$. The black line represents the cylinder when it is stationary, while the red and blue lines represents the Galilean and Franklin transformations respectively. In comparison to the previous result, the effect of the rotating very good conducting cylinder in the case of dispersive material is primarily seen in the side lobes of the forward facing backscattered field. The minor shift is happening in the primary lobe. The shifting of both the primary and side lobes happened in the direction of rotation as shown in Fig 11 and 12. The Galilean transformation, like the previous result, did not exhibit the same behavior as the Franklin transformation. The effect of rotation, in the case of dispersive material, is only seen at the peak frequencies of the pulses.

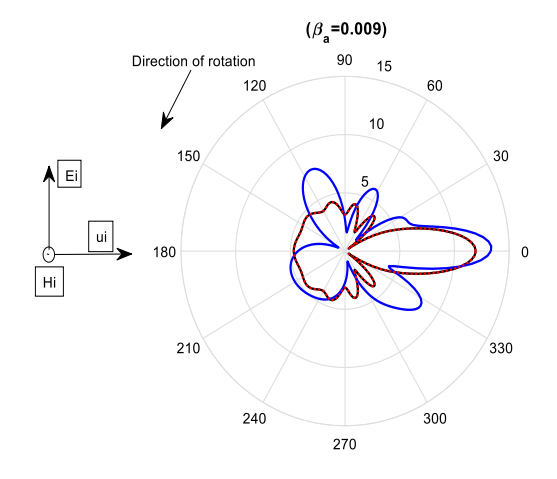


Fig. 11 Incident H-wave immersed, very good conducting cylinder $(\beta_a = 0.009)$

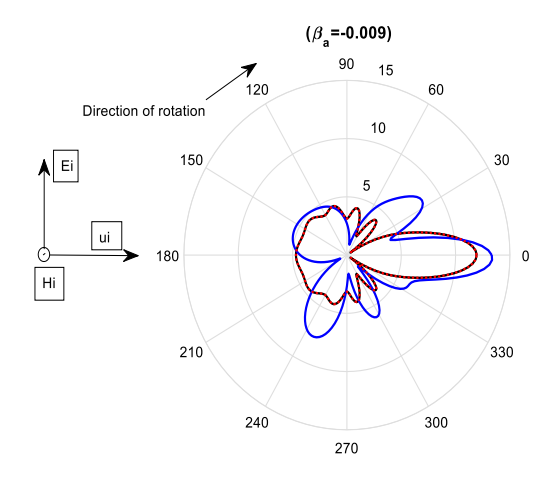


Fig.12 Incident H-wave immersed, very good conduction cylinder ($\beta_a = -0.009$)

IV. CONCLUSION

This research investigated the backscattered field of a rotating dispersive very good conducting cylinder. The cylinder was made of linear, homogenous, dispersive, and isotropic material. This investigation expands on a previous work in the case of a non-dispersive rotating very good conducting cylinder. This investigation shows that there is a difference that is more evident in the rotating case than in the stationary case. This difference can be seen more in the case of the incident H-wave than in the incident E-wave. In TE mode, this effect is shown as periodic pulses where the period of these pulses is increased when the rotation of the dispersive very good conducting cylinder is increased. Also, this period is decreased when the radius of the dispersive very good conducting cylinder is increased. In comparison to the previous work, where the results took the form of a sinusoidal wave for the backscattered phase, and the backscattered magnitude showed periodicity (especially at higher frequencies). In the case of TM-mode, there is no difference between dispersive and non-dispersive rotating very good conducting cylinders. That means the stationary case is the same as the rotation case. Future work will include investigating the effect of a moving (rotation and translation) dispersive very good conducting cylinder on the backscattered phase and magnitude. Also, a new model will be created using the backscattered field data to simulate rotation and translation.

REFERENCES

- E. Abuhdima and R. Penno, "Simulation of the scattered EM fields from a rotating conducting cylinder," IEEE International Radar, 2015.
- [2] C. A. Balanis, Advanced Engineering Electromagnetics, John Wiley &Sons, Inc, (1989).
- [3] G. Harding and R. Penno, "Dynamic Simulation of Electromagnetic Scattering from Complex Airborne Platforms," IEEE Radar Conference, Cincinnati, OH May, 2014.
- [4] Philip Franklin, "The meaning of rotation in the special theory of relativity," Proc. Nat. Acad. Sci., vol. 8, No. 9, 1922
- [5] Alessandro Alabastri and others, "Molding of Plasmonic Resonances in Metallic Nanostructures:Dependence of the Non-Linear Electric Permittivity on System Size and Temperature," materials 2013, 6, 4879-4910
- [6] Harrington, Time Harmonic Electromagnetic Fields, McGraw-Hill, 1961, pg 234.
- [7] C. T. Tai, "Two scattering problems involving moving media," Ohio State Uni. Res. Foundation, Rep. 1691-7, May 1964.
- [8] D. De Zutter, "Scattering by a rotating circular cylinder with finite conductivity,"IEEE Transactions on Antenna and Propagation, vol. AP-31, No. 1, PP. 166-169, 1983.
- [9] P. Hillion, "Scattering by a rotating circular conducting cylinder II, "Mathematical physics, vol. 41, 1998.
- [10] E. Abuhdima and R. Penno, "A Model of EM fields from Static data for Moving Conducting Cylinder," Advances in Science, Technology and Engineering Systems Journal, Volume 3, Issue 5, page No 307-310, 2018.